Alba, S. G., Jiménez, C. V., Zang, A. (2020): Evidencing the relationship between injected volume of water and maximum expected magnitude during the Puerto Gaitán (Colombia) earthquake sequence from 2013 to 2015. - *Geophysical Journal International*, *220*, 1, pp. 335—344.

DOI: http://doi.org/10.1093/gji/ggz433

Geophysical Journal International

Geophys. J. Int. (2020) **220,** 335–344
doi: 10.1093/gji/ggz433
Advance Access publication 2019 October 07
GJI Seismology

Evidencing the relationship between injected volume of water and maximum expected magnitude during the Puerto Gaitán (Colombia) earthquake sequence from 2013 to 2015

Sebastián Gómez Alba,[1,2] Carlos A. Vargas[1] and Arno Zang[3]

[1] *Geosciences Department, Universidad Nacional de Colombia, Bogotá, Colombia. E-mail: sagomezalb@unal.edu.co*
[2] *Petroleum Engineering Department, Universidad de América, Bogota, Colombia.*
[3] *German Research Center for Geosciences GFZ, Section 2.6 Seismic Hazard and Risk Dynamics, Potsdam, Germany*

Accepted 2019 September 13. Received 2019 September 5; in original form 2018 December 3

ABSTRACT

Since 2013 to date more than 1000 seismic events have been recorded by the Servicio Geologico Colombiano (Colombian Geological Survey, SGC) in the municipality of Puerto Gaitán (Colombia). A total of 14 earthquakes are moment magnitude $M_w > 4.0$. The largest event ever recorded in the area occurred in November 2015 with M_w 4.8. It seems like the case of Puerto Gaitán is associated with the deep injection of coproduced wastewater from oil and gas extraction. The data presented in this work suggests a close relationship in space and time between injection operations and seismicity. An analysis of temporality between both data sets resulted in a time lag equivalent to about 218 d. For this paper, we computed the input and output energy during injection operations from 2013 to 2015 in order to estimate the fraction of total input energy that is radiated as seismic waves. Our results suggest that the seismic energy is only a small fraction of the total energy into the system. Although Puerto Gaitan is one of the places with the most significant volume of wastewater injected among the ones reported in the literature, the energy efficiency of the system is the lowest reported to date in comparison with other applied technologies. The low efficiency seems to be associated to the aseismic deformation of the reservoir rocks. The observed clustering of earthquakes is delimited by the basement crystalline depth. From an operational point of view, we determine that, like most cases associated with fluid injection, volume of fluid is the variable that determines change in the seismic moment released. Furthermore, the sequence of events in Puerto Gaitán may not fit into a well-known correlation between the volume of fluid injected and the maximum expected magnitude. The observed magnitudes in Puerto Gaitan are well bellow compared to those reported in the literature for similar volumes of injected fluid.

Key words: Earthquake interaction, forecasting, and prediction; Induced seismicity; Seismicity and tectonics.

1 INTRODUCTION

Since early to mid-20th-century the Anthropogenic Seismicity (AS) in North America and Europe has been related to underground fluid injections and productions (Ellsworth 2013). There is a general consensus in accepting that AS is generated by two main causes: an increase in pore-fluid pressure and/or a change in the state of the stress that may cause reactivation of existing faults or fractures (Healy *et al*. 1968; Raleigh *et al*. 1976). Recent case studies suggest that fluid-induced seismicity results from wastewater disposal (Ellsworth 2013; Keranen *et al*. 2014), hydraulic fracturing (Bao & Eaton 2016), CO_2 sequestration (White & Foxall 2016), gas storage and extraction (Cesca *et al*. 2014) and geothermal energy (Cornet 2016; Lengliné *et al*. 2017). In the United States the magnitude and frequency of occurrence of induced earthquakes has increased considerably during the last decades. For instance, in the state of Oklahoma (USA) the injection of waste water associated with the extraction of shale gas, has caused earthquakes with magnitudes up to $M_w = 5.8$. Moreover, the annual earthquake rate of $M_w > 3.0$ has increased from 1.6/yr to 850/yr in 2015 (Keranen *et al*. 2014). Some examples of earthquakes that are suspected to be associated with geothermal activity are those registered in the city of Basel (Switzerland) and Pohang (South Korea). The first was $M_w = 3.4$ (Mukuhira *et al*. 2013) and the second $M_w = 5.4$ (Grigoli *et al*. 2018; Kim *et al*. 2018), both in regions considered to have very low seismic activity. The seismicity associated to hydraulic fracturing of sedimentary rocks during shale gas extraction operations, generates very small magnitude earthquakes, compared to those associated with the injection of wastewater or geothermal energy (Davies *et al*. 2013).

McGarr (1976, 2014) established a mathematical relationship that shows a proportional increase between the induced seismic moment (M_O) and the volume of injected fluid (V). Some other studies have shown that M_O depends on $V^{3/2}$ rather than on V (Galis *et al*. 2017). Schultz *et al* (2018) and Eaton & Igonin (2018) came to this last reasoning by comparing the released M_O of induced events with the injected fluid volume in Canada. One more study based on statistical analysis of the seismogenic index (Shapiro *et al*. 2010), also established that M_O depends on $V^{3/2b}$, where b is the Gutenberg–Richter exponent (Van der Elst *et al*. 2016). There is a general consensus that the volume of fluid V is the main parameter to estimate the M_O released during injection operations. However, additional case studies have discussed the role of other operational parameters different from V to influence the likelihood of induced seismic events during wastewater fluid injection (Weingarten *et al*. 2015), which include the injection rate (Frohlich 2012; Keranen *et al*. 2014), the wellhead injection pressure (Block *et al*. 2014), the proximity of the injection depth to the crystalline basement (Kim 2013), the state of stress at reservoir depth (Zang *et al*. 2014), and poroelastic stress (Goebels *et al*. 2017).

In this study, we focus on estimating the seismic energy efficiency during wastewater injection operations in Colombia's most productive heavy oilfield from 2013 to 2015 in the municipality of Puerto Gaitan. We have first collected data from simultaneously measurements of injected volume, fluid surface pressure and flow injection rate provided by the Agencia Nacional de hidrocarburos (Hydrocarbon National Agency of Colombia, ANH), and the catalogue of earthquakes recorded by the SGC. Based on those measurements, we then assessed the relationship between the radiated seismic energy E_S and pumped-in hydraulic energy E_{PH}. Through our research, we show that E_S constitutes only a small fraction of the total input energy confine within the rock volume. It was also found that it is the reservoir with the lowest energy efficiency compared to other applied technologies, despite being one of the places with the largest volume of fluid injected among those reported in the literature to date.

2 SEISMICITY AND WASTEWATER INJECTION SCENARIO

Seismotectonic context of Colombia

Colombia is located in the northwestern corner of South America. This region is characterized by a continental deformation that has evolved and made its current geological and tectonic settings through a complex history. Nowadays the state of stress is determined by the movement of Nazca and Caribbean plates to South America in direction W–E and NNW–SSE, respectively; as well as the presence of several tectonic blocks (Cediel *et al*. 2003). At present the main processes of crustal deformation are geographically framed within the Andean region. Fig. 1(a) shows the main fault systems in the country as well as the direction of relative movement Nazca, Caribbean and South America of tectonic plates. It also shows the distribution of the shallow seismicity in Colombian territory reported by SGC from 1993 to 2016 with depths ranging within 0–40 km and magnitudes $M_L > 2.0$. The natural seismic activity in the country is associated with this fault system and plates interaction. It is possible to identify surficial events along the Pacific Coast and the Colombian trench due to the subduction of the Nazca Plate (Taboada *et al*. 2000; Cediel *et al*. 2003; Vargas & Mann 2013). The seismicity at the north appears very diffuse, given the low rate of convergence between the Caribbean and the South American Plate, where crustal deformation has not reached a high state to generate significant seismic activity (Taboada *et al*. 2000). There are also events clusters within the territory associated to the Andean fault system. Another feasible feature of shallow seismicity occurs at the eastern foothills of the Eastern Cordillera, where crustal deformation is very high (Mora *et al*. 2010). Heading east, a seismic nest appears in the middle of the Eastern Llanos Basin. The seismicity at the east has been reported as non-existent over time, so it has not been possible to associate it to current tectonic activity in the region, but a sequence of possible induced seismic activity has been associated with increases in oil production (Gómez-Alba *et al*. 2015).

Seismic network and data

Unlike other studies on anthropogenic seismicity, where the information comes from records of dense networks located around the study areas, this one uses records from a regional network. Distances between epicentres events and stations can reach in some cases to up to tens of kilometres. The NSNC is composed by 52 seismological digital stations deployed throughout the NW corner of South America. Due to the high concentration of seismic activity at the west and central regions of the country most of stations are placed there. All local events were located by using the SEISAN package (Havskov & Ottemöller 2000) and the algorithm HYPOCENTER (Liener & Havskov 1995). The velocity model used for the location is an average 1-D model for Colombia that consists of six layers (Ojeda & Havskov 2001).

Induced seismicity in Puerto Gaitan

Fig. 1(b) shows the distribution of closest seismological stations to Puerto Gaitan, spatiotemporal distribution of earthquakes from 1993 to 2017 and injection clusters. From 1993 to 2011 the number of events recorded in the study area was 10. As of 2012 and until the end of 2013 the number of earthquakes increased to 110. Due to the unexpected increase in recorded events, the SGC deployed the seismological station of Puerto Gaitán (PTGC) in September 2013. During 2014 and 2015 the SGC registered a total of 804 events. Between 2016 and 2017 the number of earthquakes decreased to 149. Regarding the spatial distribution, it can be seen that after 2013 a large number of events spread to the northwest from the original cluster. After 2016 earthquakes regroup again around epicentral solutions registered back in 2013. The SGC recorded a total number of 1108 events in Puerto Gaitan. Catalogue of earthquakes (Annex 1) shows that average earthquake depth is 3.62 km. Around 940 events are located between 0 and 4 km in depth. Regarding magnitudes, it was established that average M_w is 3.47, from which 14 earthquakes are $M_w + 4.0$.

Data from 51 injection wells grouped into eight clusters distributed throughout the largest heavy oil producing field in Colombia were considered in this study. It was determined that in March 2013 the cumulative injected water was close to 2.1×10^8 (m^3). By the end of 2015, the cumulative volume of injected water reached 7.0×10^8 (m^3). It was also established that some injection wells started operations 1492 d before to March 2013 (Annex 2).

A qualitative analysis suggests that cumulative M_O (Nm) and V (m^3) curves have similar shapes but are out of phase in time

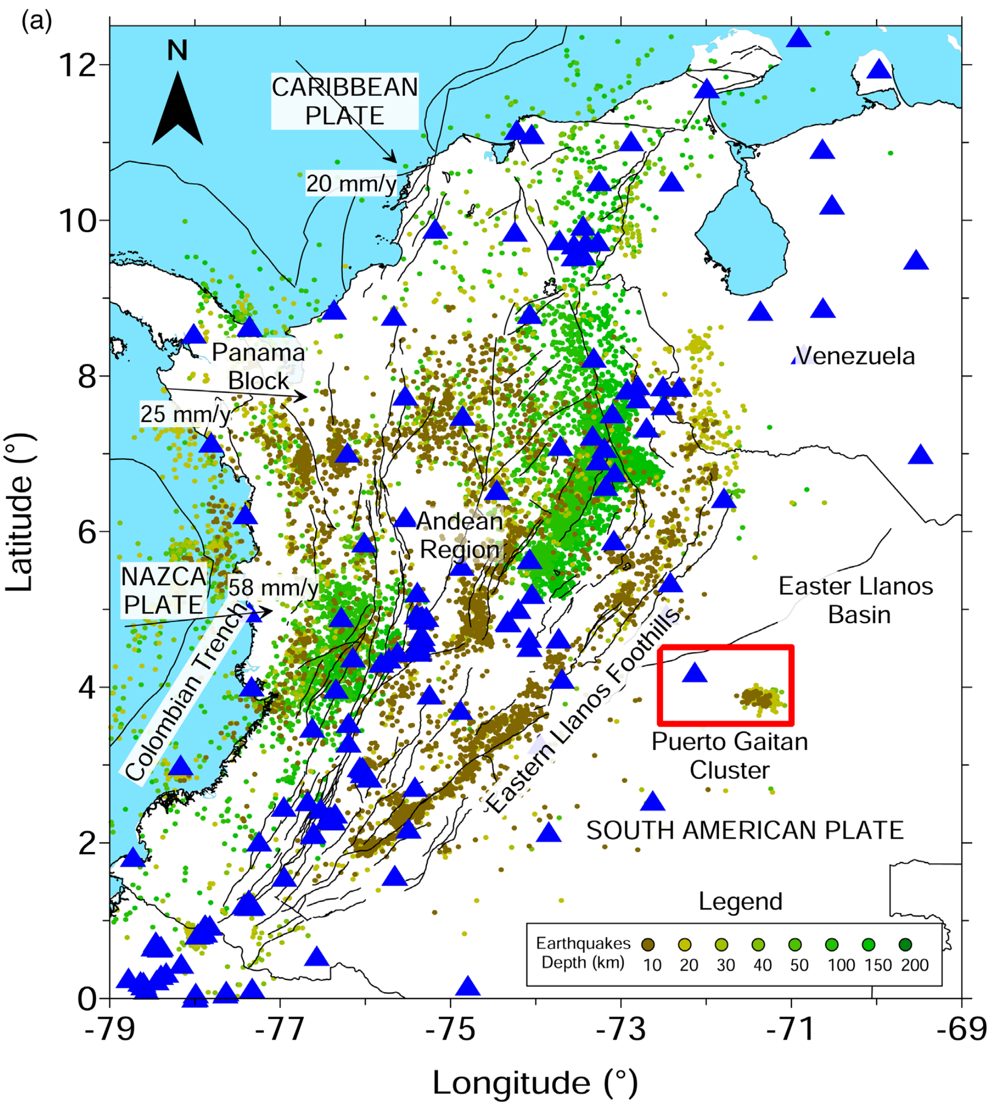

Figure 1. (a) Seismotectonic context of Colombia. The figure shows the configuration of the tectonic system of the NW corner of South America (interaction between the Nazca, Caribbean and South America plates). Additionally, the interaction of microplates or blocks, as is the case of the Panama Block. The arrows represent the relative movement of the Nazca and Caribbean plates, and the Panama Block with respect to the South American Plate. The black lines represent the distribution of the most important fault systems that run through the country and that are mostly associated with the mountain system of the Andes. Seismicity is represented by coloured circles in function of depth. The seismicity distribution is mostly associated with deformation and failure processes in the Andes and Colombian trench on the Pacific Ocean. To the east, in the Eastern Llanos Basin the events cluster of Puerto Gaitan is highlighted in a red square. The blue triangles represent the distribution of the seismic network deployed by the Colombian Geological Service (SGC).

(Fig. 2a). When the V curve increases, the cumulative M_O curve also does so time later. Analagogically, when V curve does not increase, the upturn of cumulative M_O curve stabilizes. To determine the time lag between both curves, we performed a cross-correlation between both time-series curves and determined that the maximum lag between them is approximately 218 d (Fig. 2b).

3 METHODOLOGY

To be able to compare both sets of data with each other, we converted injection and seismicity in terms of energy. The following paragraphs describe the energy calculations and the parameters extracted from each stage in order to determine these values.

Pumped-in hydraulic energy E_{PH}: The injection energy was calculated to define the total input energy available to perform the waste water injection. Since the pumping data at the surface is available, the total input energy can be calculated by using the following equation:

$$E_{PH} = \int_{t1}^{t2} PQdt \approx \langle P(t)\rangle \langle Q(t)\rangle \Delta t \ ,$$

where t_1 and t_2 are the start and end times of the injection procedure. $\langle P(t)\rangle$ and $\langle Q(t)\rangle$ denotes the monthly average of surface injection pressure (MPa) and injection rate (m^3/s) of the total number of injection wells. Δt is the total duration of the water injection cycle.

Radiated seismic energy E_S: The radiated seismic energy was calculated to determine how much of the output energy was contributed by the recorded events. This is given in units of Joules by:

$$\log_{10}(\mathrm{Es}) = 1.5\mathrm{Mo} + 4.8$$

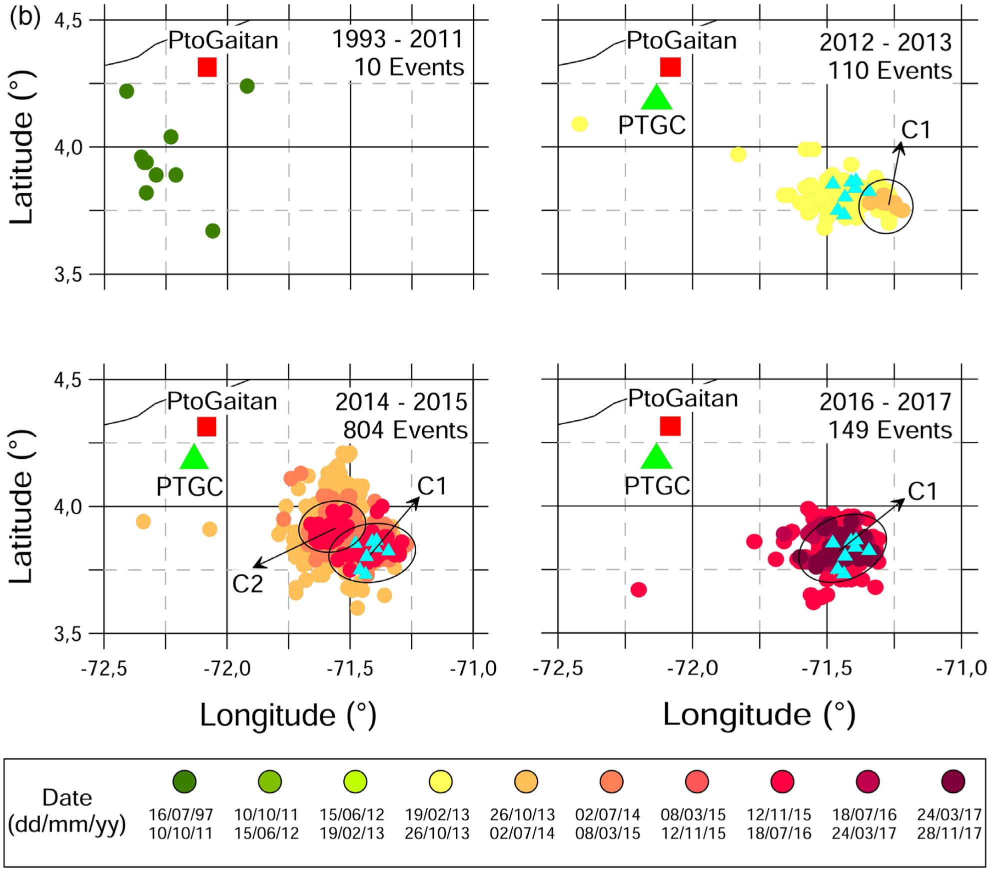

Figure 1. (b) Seismicity distribution in Puerto Gaitan. Each panel shows the distribution of seismicity in Puerto Gaitán as a function of time from 1993 to 2017. The red square represents the location of the city of Puerto Gaitán, and the green triangle is the closest seismological station to the study area (PTGC). The largest number of recorded events took place between 2014 and 2015, with a total of 804 events. The blue triangles represent the 8 injection clusters, which group a total of 51 injection wells. Given the proximity between the events and the injection wells, the seismicity has been catalogued as human related.

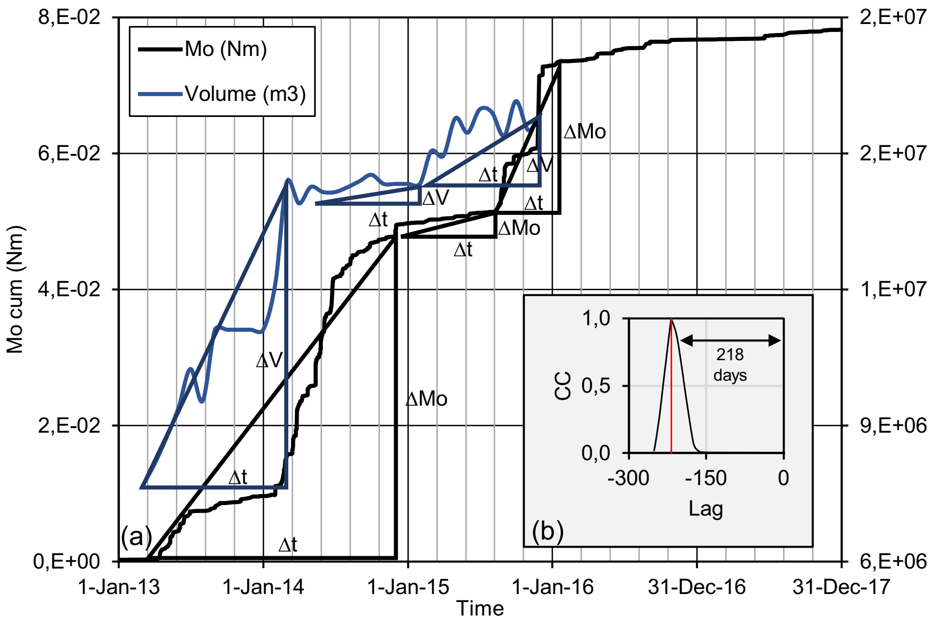

Figure 2. Relationship between seismicity and water injection curves. Data sets have similar shapes but out of phase in time. (a) The blue line and black line represent Water Injection, V, (m^3) and seismic moment, M_O, (Nm), respectively. Slopes are a schematic representation of input energy into the system ($\Delta V/\Delta t$) and output energy from the system ($\Delta M_O/\Delta t$). (b) Cross-correlation between both injection and seismic moment curves from Fig. 2(a). Red line shows the lag at maximum correlation. Maximum lag is ~218 d.

This equation is modified from Kanamori (1977), who used the Gutenberg–Richter magnitude energy relation calibrated for large earthquakes and expressed the result in units of ergs. M_O denotes seismic moment and was computed using the following equation:

$$M_w = \left(2/3\right) \log_{10}(M_O) - 6$$

Finally, E_S is computed by adding the energy for all recorded earthquakes after converting the reported moment magnitudes into energy based on scaling relations developed in earthquake seismology.

To estimate both E_{PH} and E_S we considered some assumptions. For instance, due to the proximity of injection wells we assumed it was reasonable to add all volumes from wells to obtain the total injected volume. The time windows in Puerto Gaitán are not decades old, and the distances are not significant either, so the sum of all the volumes of water is totally adequate. We considered that taking the pressure and injection averages was also acceptable. We also assumed that all seismicity in the area was human related. The above is based on the historical seismicity in the regional context, which we consider as nonexistent before 2013. Furthermore, a suitable distance radius to determine if an event can be induced due to the injection of water at any time after the start of the injection, is ∼20 km according to correlations observed in the literature for the basins of the United States (Rubinstein & Babaie Mahani 2015). The previous assumptions had to be made due to the way in which the database presents the average operation parameters. Multiple injection scenarios can be proposed and E_{PH} estimations may vary considerably between each other. Moreover, E_S inaccuracies may be also considered since the radiated seismic energy relations are calibrated for large earthquakes ($M_w > 3.5$) and in this study are applied to events that are some magnitudes smaller.

In order to determine how reliable the recording capability of the network is we performed an analysis of M_c and *b*-value over time (Fig. 3). M_c was estimated by defining the point of the maximum curvature (MAXC). This value is obtained by computing the maximum value of the first derivate of the frequency magnitude curve. In practice, this matches the magnitude bin with the highest frequency of events in the non-cumulative frequency magnitude distribution (Wiemer & Wyss 2000). To estimate the *b*-value we used a maximum-likelihood technique (Aki 1965; Bender 1983):

$$b = \frac{\log_{10}(e)}{\left[\langle M\rangle - \left(M_c - \frac{\Delta M_{\mathrm{bin}}}{2}\right)\right]},$$

where ⟨M⟩ is the mean value of the magnitudes greater or equal to M_c, and $\Delta M_{\mathrm{bin}} = 0.1$ is the binning width of the catalogue. The analysis was performed for a total of 7 periods, each with a total of 158 events. The *b* parameter characterizes the ratio of the number of stronger earthquakes to the number of weaker ones, and its value vary from 0.5 to 1.5 depending on the distribution regional stress and tectonics (Mogi 1967; Tsapanos 1990). The lower the *b* coefficient, the larger the probability of have stronger events. According to Fig. 3, the largest *b*-value reported in Puerto Gaitan occurs between August 2014 and May 2015. The rest of the reported values is below 1.0, which is considered as a universal value for all tectonic regimes (Frohlich & Davis 1993; Kagan 1997, 1999; Wesnousky 1999; Godano & Pingue 2002; Bird & Kagan 2004; Wech *et al.* 2010). The probabily of occurrence of large events in Puerto Gaitan seems to be low. M_c does not vary drastically, so we consider that the recording capability of the seismic network is good enough to record events over time.

4 RESULTS: PUMPED-IN HYDRAULIC ENERGY E_{PH} AND RADIATED SEISMIC ENERGY E_S

Main results are shown in Fig. 4. The analysis was carried out for 34 periods of time, corresponding to the months between March 2013 and December 2015. To estimate the input hydraulic energy we used the monthly averages of injection rate and injection pressure. The output elastic energy was assessed by using the energy released of each individual induced event in the study area.

The upper panel (Fig. 4a) shows Q (m^3 s^{-1}) and P (MPa) over time. The injection rate (blue curve) increase steadily over time. The average injection pressure is represented by the black line. It presented two considerable fluctuations in 2013 followed by slightly more moderate variations until the end of 2015. Since both curves show average values, it is not possible to establish with certainty whether the injection of water is done in cycles or if it is done invariably. Fig. 4(b) shows the M_w and E_S of induced earthquakes. Events with $M_w > 4.0$ are marked with red stars. The graph shows two significant accumulations of events. One, during the first half of 2013, and the second throughout 2014. Events with $M_w > 4.0$ were recorded during the first half of 2014 and second half of 2015. The maximum E_S released was 0.0 6259 (MJ). Fig. 4(c) shows the rate of increase of E_{PH} over time. The total cumulative E_{PH} is 3.85E + 09 (MJ) in December 2015 and was calculated through the sum of monthly E_{PH} estimations. The cumulative total of E_S equals 0.499325 (MJ) in December 2017. The bottom panel (Fig. 3d) shows the ratio of both E_S and E_{PH} changing with time. Three pick phases of efficient seismic radiation can be identified at the beginning, in the middle and at the end of the injection cycle. In-between, two stages are identified with no very efficient seismic radiation.

5 DISCUSSION

In this paper, we observed a relation in time and space between the operations of injection of residual water and the sequence of earthquakes in Puerto Gaitán between 2013 and 2015. Previous studies had reported that the seismicity in Puerto Gaitan had its origin as a consequence heavy oil production (Gomez *et al.* 2015). At the time, the available information was that of monthly oil production. In this study, we presented the volume of water injected, the pressure and flow of surface injection, as possible operating factors that induced earthquakes in Puerto Gaitán between 2013 and 2015.

Like many induced events, we hypothesize that Puerto Gaitan earthquakes are generated in the form of swarm like clustering that migrates in space and time in line with the propagation of fluids in the porus media (Shapiro *et al.* 2002). The temporal and spatial distribution of earthquakes seems to demonstrate the prior (Fig. 1b). It can be evidenced that the oldest events tend to move away from the injection clusters as time passes. The migration of the triggered front of induced seismicity is often described by a pore pressure diffusion process. Measuring the temporal space evolution of the triggered front can allow the estimation of the hydraulic diffusivity of the porus medium (Shapiro *et al.* 1997, 2002). From the distribution of the seismicity registered by the SGC, it is not possible to identify that the migration of fluids reactivates faults or creates new fractures as a mechanism for the generation of induced events. Neither is there enough information to determine if there is a causal relationship between an specific injector well and a particular earthquake.

A qualitative analysis of the slopes of the V and released M_O curves (Fig. 2a) show that both have the same shape, that is, they evolve in the same way over time. The slopes shown in Fig. 2(a)

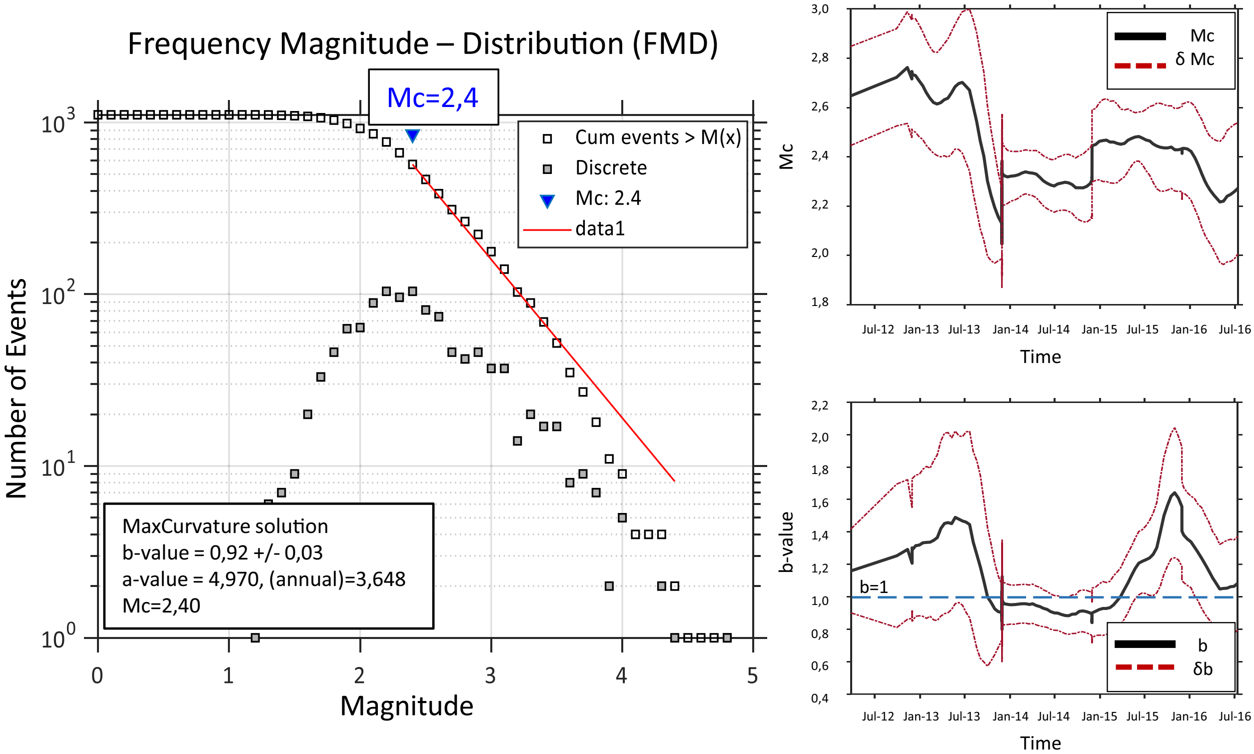

Figure 3. Cumulative frequency magnitude distribution (FMD) plots for studied data. The right-hand panels show the evolution of M_c and *b*-value over time.

of the *V* curve schematically represent the radius between $\Delta V/\Delta t$. The slopes of the released M_O curve represent $\Delta M_O/\Delta t$. Similarities between both curves were identified in three phases that were recognized. The first and the last associated with an increase in ΔV that generated an increase in ΔM_O, and an intermediate period where a decrease in ΔV was observed that triggered a decrease in ΔM_O. This feature possesses a general discussion that for the case of Puerto Gaitán, the seismicity could be purely influenced by fluids injection other than regional tectonic and stress features. One of the reasons to support this hypothesis has to do with the increase in the recorded event rate. Before 2012 this was 1/annual, when the volumes of water injected were not significant. When water volumes increased abruptly, the rate of recorded events increased to 804/annual. The second reason for this hypothesis has to do with the lag time between both curves. The 218 d established from the cross-correlation between both time-series appear to be a reasonable period for the migration front of the injected fluid volume to generate induced events (Fig. 2b). Some case studies show that this lag can occur even years after the water has been injected in tectonically stable areas like it has been the case in some areas of the United States (Chen *et al*. 2017).

The panels of Fig. 4 show the results of the conversion of the volume of water into hydraulic potential energy, and the M_O released into irradiated seismic energy. The distribution of injection pressure and flow in Fig. 4(a) allow us to identify that another possible operational factor that has an impact on the generation of induced earthquakes in Puerto Gaitan is the injection rate. The average injection rate increases steadily over time just like the M_O is released. On the contrary, the injection pressure due to observed fluctuations does not seem to be a conclusive criterion to establish the causality of the seismicity.

One of the advantages of the methodology applied in this research is that it allows to express *V* and M_O in energy units. This simplifies the assessment between both variables. Figs 4(b) and (c) show the behaviour of the input and output energy into the reservoir system over time. Fig. 4(d) shows the distribution of the radius between the output energy of the system and the input energy. The radius is not constant over time but has fluctuations that depend on the variables of operation during the injection of crude oil. We recommend to analyse this energy ratio over time for other fields of fluid-injection-induced seismicity. Peak and plateau values can be used to obtain more insights about the interrelation between seismic radiated energy and operational parameters.

We compared the seismic moment M_O released and energy efficiency of the events with M_w 4.0 + recorded in Puerto Gaitán, with other data collected worldwide in water reservoirs, during hydraulic fracturing operations, geothermal systems and laboratory experiments (Figs 5a and b). The sequence of events in Puerto Gaitán shows that released seismic moment is found to depend on the pumped-in hydraulic energy. The aforementioned means that the greater the energy injected, the greater the quantification of the energy released after the injection of fluid. There is widespread acceptance that the volume of fluid injected is the main variable to quantify the M_O released resulting from injection operations. McGarr (2014) proposes a linear relation between both parameters (M_{Otot} α *V*), while others authors such as van der Elst *et al*. (2016), Galis *et al*. (2017) and De Barros *et al*. (2019) have reported a linear relationship (M_{Otot} α $V^{(3/2)}$). It is also recognized that the prediction of M_O released from only the volume of water injected may be overestimated considering that a large part of these relationships disregard that a large part of the deformation is aseismic (De Barros *et al*. 2018; McGarr *et al*. 2018). Therefore, to assertively estimate

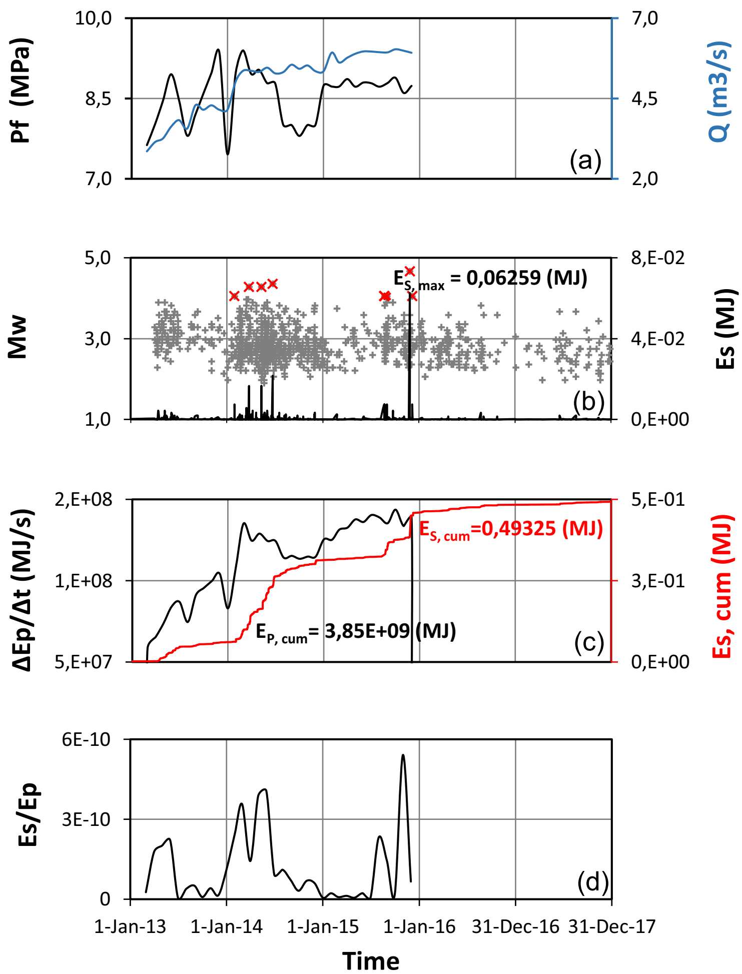

Figure 4. Input and output energy results. (a) Time variation of Injection rate (blue line) Q, ($m^3 s^{-1}$) and fluid Pressure (black line) P_f, at injection point (MPa) (b) Moment Magnitude (grey crosses), M_w and radiated seismic energy, E_S (MJ) of all sequence of induced events (black line). $E_{S,\max}$ corresponds to the highest E_S of the largest single event ($M_w = 4.8$). Red crosses are induced events with $M_w > 4.0$. (c) Time variation of rate of pumped-in hydraulic energy (black line), E_P (MJ) and cumulative radiated seismic energy (red line) $E_{S,\mathrm{cum}}$ (MJ). The area under the black curve represents the total amount of pumped-in energy $E_{P,\mathrm{cum}}$ (MJ). (d) Ratio of E_S to E_P changing with time.

the prediction of the released seismic energy, if the geological structures will respond seismically or not must be taken into account. Additionally, the sensitivity of the M_O induced to the monitoring parameters during the manipulations of industrial fluids in reservoirs should be explored. As mentioned above, an energy efficiency analysis would be a proper evaluation parameter.

Puerto Gaitan seems not to fit with the reported observations in the literature. While the volume of water in our study area surpasses those reported in documented cases, the magnitudes observed are well below the upper bound proposed by McGarr (Fig. 5a). Fig. 5(b) shows the relationship between E_{PH} versus E_S of the data shown in Fig. 5(a) and other data collected during hydraulic fracturing operations in Canada and laboratory tests. Energy efficiency during the wastewater injection cycle in Puerto Gaitán is the lowest reported among the cases documented in this study except for Groß-Schönebeck case study in Germany (number 17). The only case that has shown an efficiency close to 100 per cent is Denver. The energy ratio for the other cases is very similar. In most cases, the seismic energy released does not exceed 5 per cent of the injected energy. The efficiency in Puerto Gaitán is well below 0.0001 per cent, which indicates that the energy injected into the system is strongly dissipated during the injection cycle, and the expected seismic energy is not released.

The results obtained can be explained by two possible causes. From the point of view of the reservoir, one cause has to do with the aseismic response of the disposal reservoir. That is to say that the deformation in the disposal reservoir does not always generate an earthquake, but only a small portion of the potential energy stored in a reservoir through injection is released through brittle deformation with associated radiation of seismic energy (McGarr 2014). Another explanation may be associated with the gemoetry of fluid propagation and the diffusion of fluid pressure in the reservoir. Studies carried out by Dieterich *et al* (2015), have estimated that the escalation between M_O and V is determined by the systems of formation faults, permeability and 3-D diffusion through the Bulk. In the case of Puerto Gaitan it is possible that fraction of V is damped/filtered through fractures that connect with deeper structures of the crystalline basement and is not confined solely in the reservoir. Fig. 6 gives an independent support for this hypothesis based on gravity data inversion (Graterol & Rey 2009). Injection

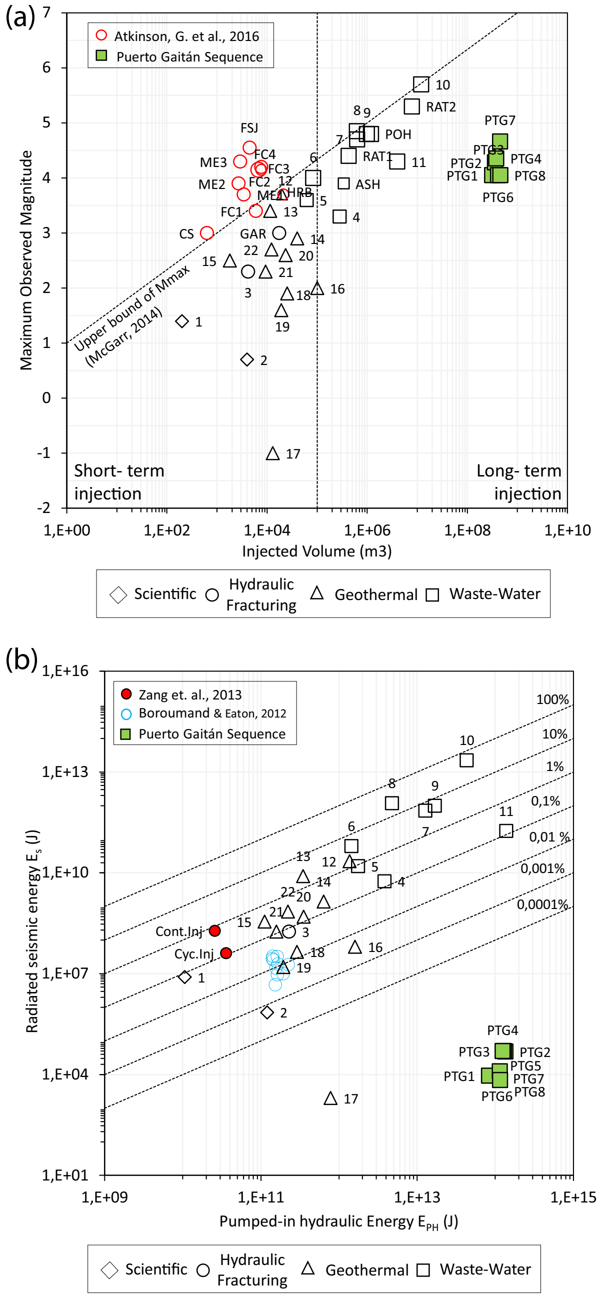

Figure 5. (a) Relationship between maximum observed seismic magnitudes and fluid volume injected during different technology operations. Symbols indicate technology type. Numbers and characters correspond to studies listed by Zhang *et al*. (2014). Red circles indicate calculations from shale gas reservoirs in Western Canada Sedimentary Basin (Atkinson *et al*. 2016): (CS) Cardston swarm, (FC1) Fox Creek event 1, (FC2) Fox Creek event 2, (FC3) Fox Creek event 3, (FC4) Fox Creek event 4, (ME1) Montney event 1, (ME2) Montney event 2, (ME3) Montney event 3, (HRB) Horn River Basin, (FSJ) Fort St. John. Upper bound is the linear relationship postulated by McGarr (2014). Green squares show the relationship between injected volume and observed magnitude for waste water induced events $M_w > 4.0$ reported in this study (PTG) Puerto Gaitán. (b) Relationship between total pumped-in energy, E_{PH}, and total radiated seismic energy, E_S. Numbers and Characters correspond to the same database used in Fig. 4(a). Blue circles indicate calculations from shale gas reservoirs (hydraulic fracturing) that are based on all induced events (Boroumand & Eaton 2012). Red circles show two stimulation models for continuous and cyclic injection procedures by Zang *et al*. (2013). The dotted lines represent the energy efficiency.

clusters and earthquakes are located on a structural high where we assume the crystalline basement to be superficial and gravity data is higher. To the southeast and northwest we find two depocenters where no seismic activity has been recorded. It seems that earthquakes are grouped in areas where the basement is shallower. The experience of large scale wastewater injection in Oklahoma (USA) shows that seismicity occurs mainly in the highest part of the crystalline basement. McNamara *et al*. (2015), state that earthquakes in Oklahoma are due to the reactivation of subsurface faults that extend into the crystalline basement. Similar observations have also taken place in CO_2 injection operations at Decatur, Illinois (Goertz-Allmann *et al*. 2017). The Puerto Gaitan basement seems to play two fundamental roles: the first one is to set the seismicity in the current cluster of events in the structural high, that is, when the basement is shallow. The second role has to do with the possible hydraulic connection (permeability) of faults that allow the percolation of water in deeper structures, precisely where the basement is deeper and where the seismicity has not yet spread. Adequate mitigation of risk in Puerto Gaitan, and in general of areas where long-term Injection experimets are made, requires the prior mapping of faulted structures with hydraulic connection between the disposal reservoir and the crystalline basement.

6 CONCLUSIONS

The relationship between oilfield operations and seismicity between 2013 and 2015 in the municipality of Puerto Gaitán is suggestive. Our analysis and results propose that the sequence of events in Puerto Gaitán are the result of the release of the elastic energy stored in the reservoir due to the continuous action of the work exerted by the injection of water. The released M_O in Puerto Gaitan depends on the injected volume, but also on injection rate, surface pressure, depth of crystalline basement and stress conditions of the reservoir. Establishing the relationship between the previous operative criteria and M_O are necessary for understanding and control of long-term injection experiments in the field. The behaviour of the V and M_O curves in Puerto Gaitan show us that a reduction of the total pumped volume or slow injection operations may reduce seismic hazard in the area. A hydromechanical analysis allows us to determine that the energy efficiency of the injection cycle is well compared to other documented long-term injection operations. The high seismic deformation of the reservoirs and the possible filtration of large volumes of fluid injected into deeper structures are the main causes that generate low energy efficiency in Puerto Gaitan. These two conditions have allowed long-term injection of large volumes to have not lead to significant larger events. However, it is essential to settle if there is a hydraulic connection (high permeability) between the reservoir and the crystalline basement, most likely through basement faults reaching into the reservoir.

ACKNOWLEDGEMENTS

We want to thank NEXCOA Workshop funding for bringing us together. This work is partially supported by the Universidad Nacional de Colombia, Departamento de Geociencias. S. Gómez-Alba thanks a fellowship by COLCIENCIAS (Grant: Doctorados Nacionales 617-2). C.A Vargas thanks to COLCIENCIAS for partial funding through grant FP44842-006-2016 (Análisis 4-D de Vp, Vs y la relación Vp/Vs en la Esquina NW de Suramérica). We wish to acknowledge the work of the Colombian Geological Survey (SGC)

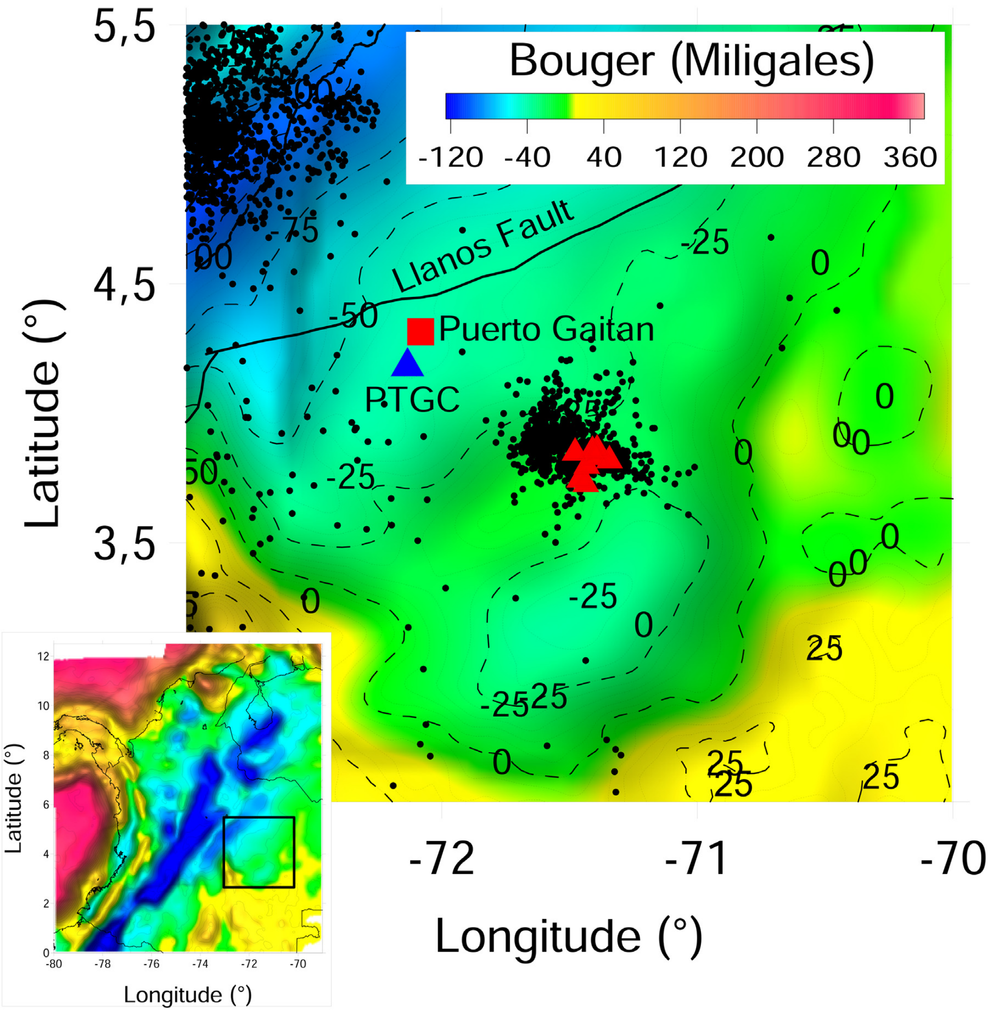

Figure 6. Inversion map of gravity data for Colombia. Seismic events and Injection clusters are set at a structural height. The events are distributed northwest of the study area. To the south where the basement is deeper there has not been seismic activity recorded until to date (modified from Graterol & Rey 2009).

for providing the seismological data, as well as the National Hydrocarbon Agency (ANH) for providing water injection information. Comments from Editor Professor Gabi Laske, reviewer Volkey Oye and one more anonymous reviewers are acknowledged.

REFERENCES

Aki, K., 1965. Maximum likelihood estimate of b in the formula log N = a - b M and its confidence limits, *Bull. seism. Soc. Am.*, **43,** 237–239

Atkinson, G.M., Eaton, D.W., Ghofrani, H., Walker, D., Cheadle, B., Schultz, R. & Liu, Y., 2016. Hydraulic fracturing and seismicity in the Western Canada Sedimentary Basin, *Seismol. Res. Lett.,* **87,** 631–647.

Bao, X. & Eaton, D.W., 2016. Fault activation by hydraulic fracturing in western Canada, *Science,* **354**(6318), 1046–1409.

.Barros, L, Cappa, F., Guglielmi, Y., Duboeuf, L. & Grasso, J.R., 2019. Energy of injection-induced seismicity predicted from in-situ experiments, *Scientific Reports,* **9,** 10.1038/s41598-019-41306-x

Bender, B., 1983. Maximum likelihood estimation of b values for magnitude grouped data, *Bull. seism. Soc. Am.,* **73,** 831–851.

Bird, P & Kagan, Y, 2004. Plate-Tectonic Analysis of Shallow Seismicity: Apparent boundary Width, Beta, Corner Magnitude, Coupled Lithosphere Thickness, and Coupling in Seven Tectonic Settings, *Bull. seism. Soc. Am.,* **94** (6), 2380–2399.

Block, L.V., Wood, C.K., Yeck, W.L. & King, V.M., 2014. The 24 January 2013 ML earthquake near Paradox, Colorado, and its relation to deep well injection, *Seismol. Res. Lett.,* **85**(3), 609–624.

Boroumand, N. & Eaton, D.W., 2012 Comparing energy calculation: hydraulic fracture and Microseismic monitoring, in *Proceedings of the Geo-Convention: Vision,* Calgary, Canada, 14–18 May 2012.

Cediel, F., Shaw, R.P. & Caceres, C., 2003. Tectonic assembly of the northern Andean block, in The circum-Gulf of Mexico and the Caribbean: Hydrocarbon habitats, basin formation, and plate tectonics, *AAPG Mem.,* **79,** 1–34.

Cesca, S. *et al.*, 2014. The 2013 September–October seismic sequence offshore Spain: a case of seismicity triggered by gas injection? *Geophys. J. Int.,* **182**(2), 941–953.

Chen, X. *et al.*, 2017. The Pawnee earthquake as a result of the interplay among injection, faults and foreshocks, *Sci. Rep.,* **7**. doi:10.1038/s41598-017-04992-z.

Cornet, F.H., 2016. Seismic and aseismic motions generated by fluid injections, *Geomech. Ener. Environ.,* **5,** 42–54.

Davies, R., Foulger, G., Bindley, A. & Styles, P., 2013. Induced seismicity and hydraulic fracturing for the recovery of hydrocarbons, *Mar. Petrol. Geol.,* **45,** 171–185

De Barros, L., Guglielmi, Y.D., Cappa, F. & Duboeuf, L., 2018. Seismicity and fault aseismic deformation caused by fluid injection in decametric in-situ experiments, *Comptes Rendus Geoscience,* **350** (8), 464–475.

Dieterich, J.H., Richards-Dinger, K.B. & Kroll, K.A., 2015. Modeling injection-induced seismicity with the physics-based earthquake simulator RSQSim, *Seismol. Res. Lett.,* **86**(4), 1102–1109.

Eaton, D.W. & Igonin, N., 2018. What controls the maximum magnitude of injection-induced earthquakes? *Leading Edge,* **37**(2), 135–140.

Ellsworth, W., 2013. Injection-induced earthquakes, *Science,* **341,** 1225942.

Frohlich, C., 2012. Two-year survey comparing earthquake activity and injection-well locations in Barnett Shale, Texas, *Proc. Natl Acad. Sci. USA,* **109,** 13934–13938

Frohlich, C. & Davis, S., 1993. Teleseismic b-values: or, much ado about 1.0, *J. geophys. Res.,* **98,** 631–644.

Galis, M., Ampuero, J.P., Mai, P.M. & Cappa, F., 2017. Induced seismicity provides insight into why earthquake ruptures stop, *Sci. Adv.,* **3**(12), .

Godano, C. & Pingue, F., 2002. Is the seismic moment-frequency relation universal?, *Geophys. J. Int.,* **142,** 193–198, 10.1046/j.1365-246x.2000.00149.x.

Goebels, T.H.W, Weingartenb, M., Chenc, X., Haffenerc, J. & Brodskya, E.E., 2017. The 2016 Fairview Oklahoma earthquakes: Evidence for long-range poroelastic stress triggering at >40 km from fluid disposal wells, *Earth planet. Sci. Lett.,* **472,** 50–61.

Goertz-Allmann, B.P., Gibbons, S.J., Oye, V., Bauer, R. & Will, R., 2017. Characterization of induced seismicity patterns derived from internal structure in event clusters, *J. geophys. Res.,* **122,** 3875–3894.

Graterol, V. & Rey, C.A., 2009. Mediciones aerogravimétricas y magnetométricas en los Llanos Orientales de Colombia, X Simposio Bolivariano Exploración Petrolera en Cuencas Subandinas, Cartagena, Colombia.

Grigoli, F. *et al.*, 2018. The November 2017 Mw 5.5 Pohang earthquake: a possible case of induced seismicity in South Korea, *Science,* **360**(6392), 1003–1006.

Gómez-Alba, S., Fajardo-Zarate, C.E. & Vargas, C.A., 2015. Stress field estimation based on focal mechanisms and back projected imaging in the Eastern Llanos Basin (Colombia), *J. S. Am. Earth Sci.,* **71,** 320–332, .

Havskov, J. & Ottemoller, L., 2000. *The SEISAN Earthquake Analysis Software,* Institute of solid Earth Physics University of Bergen, Bergen, Norway, p. 250

Healy, J., Rubey, W., Griggs, D. & Raleigh, C., 1968. The Denver earthquakes, *Science,* **161,** 1301–1310.

Kagan, Y.Y., 1997. Seismic moment-frequency relation for shallow earthquakes:regional comparison, *J. geophys. Res.,* **102,** 2835–2852, doi:10.1029/96JB03386.

Kagan, Y.Y., 1999. Universality of the seismic moment-frequency relation, *Pure appl. Geophys.,* **15,** 537–573.

Kanamori, H., 1977. The energy release in great earthquakes, *J. geophys. Res.,* **82** (20), 2981–2987.

Keranen, K.M., Weingarten, M., Abers, G.A., Bekins, B.A. & Ge, S., 2014. Sharp increase in central Oklahoma seismicity since 2008 induced by massive wastewater injection, *Science,* **345**(6195), 448–451.

Kim, K.H., Ree, J.H., Kim, Y.H., Kim, S., Kang, S.Y. & Seo, W., 2018. Assessing whether the 2017 Mw 5.4 Pohang earthquake in South Korea was an induced event, *Science,* **360**(6392), 1007–1009.

Kim, W.Y., 2013. Induced seismicity associated with fluid injection into deep well in Youngstown, Ohio, *J. geophys. Res.,* **18,** 3506–3518.

Lengliné, O., Boubacar, M. & Schmittbuhl, J., 2017. Seismicity related to the hydraulic stimulation of GRT1, Rittershoffen, France, *Geophys. J. Int.,* **208**(3), 1704–1715.

Liener, B.R. & Havskov, J., 1995. A computer program for locating earthquakes locally, regionally and globally, *Seismol. Res. Lett.,* **66**(5), 26–36.

McGarr, A., 1976. Seismic moments and volume changes, *J. geophys. Res.,* **81**(1):1487–1494.

McGarr, A., 2014. Maximum magnitude earthquakes induced by fluid injection, *J. geophys. Res.,* **119,** 1008–1019.

McGarr, A. & Barbour, A.J., 2018. Injection-induced moment released can also be aseismic, *Geophys. Res. Lett.,* **45**(11)5344–5311.

McNamara, D. *et al.*, 2015. Efforts to monitor and characterize the recent increasing seismicity in central Oklahoma, *Lead. Edge,* **34**(6), 628–639.

Mogi, K., 1967. Regional variation in magnitude-frequency relation of earthquake, *Bull. Earthq. Res. Inst.,* **45,** 313–325.

Mora, A., *et al.*, 2010. The eastern foothills of the eastern cordillera of Colombia: an example of multiple factors controlling structural styles and active tectonics, *Bull. Geol. Soc. Am.,* **122** (11–12), 1846–1864.

Mukuhira, Y., Asanuma, H., Niitsuma, H. & Häring, M.O., 2013. Characteristics of large-magnitude microseismic events recorded during and after stimulation of a geothermal reservoir at Basel, Switzerland, *Geothermics,* **45,** 1–17.

Ojeda, A. & Hasvkov, J., 2001. Crustal structure and local seismicity in Colombia, *J. Seismol.,* **5**(4) 575–593

Raleigh, C., Healy, J. & Bredehoeft, J., 1976. An experiment in earthquake control at Rangely, Colorado, *Science,* **191,** 1230–1237.

Rubinstein, J.L. & Babaie Mahani, A., 2015. Myths and Facts on Wastewater Injection, Hydraulic Fracturing, Enhaced Oil Recovery, and Induced Seismicity, *Seismol. Res. Lett.,* **86,** 1060–1067, 10.1785/0220150067 .

Schultz, R., Atkinson, G., Eaton, D.W., Gu, Y.J. & Kao, H., 2018. Hydraulic fracturing volume is associated with induced earthquake productivity in the Duvernay play, *Science,* **359**(6373), 304–308.

Shapiro, S.A., Dinske, C., Langenbruch, C. & Wenzel, F., 2010. Seismogenic index and magnitude probability of earthquakes induced during reservoir fluid stimulations, *Leading Edge,* **29**(3), 304–309.

Shapiro, S.A., Huenges, E. & Borm, G., 1997. Estimating the crust permeability from fluid-injection-induced seismic emission at the KTB site, *Geophys. J. Int.,* **131**(2), F15–F18.

Shapiro, S.A., Rothert, E., Rath, V. & Rindschwentner, J., 2002. Characterization of fluid transport properties of reservoirs using induced microseismicity, *Geophysics,* **67,** 212–220.

Taboada, A., Rivera, L.A., Fuenzalida, A., Cisternas, A., Philip, H., Bijwaard, H., Olaya, J. & Rivera, C., 2000. Geodynamics of the Northern Andes; subductions and intracontinental deformation (Colombia), *Tectonics,* **19,** 787–813.

Tsapanos, T., 1990. b-Value of two tectonic parts in the circum-Pacific belt, *Pure appl. Geophys,* **143,** 229–242, doi: 10.1007/BF00876999.

van der Elst, N.J., Page, M.T., Weiser, D.A., Goebel, T.H.W. & Hosseini, S.M., 2016. Induced earthquake magnitudes are as large as (statistically) expected, *J. geophys. Res.,* **121,** 4575–4590.

Vargas, C.A. & Mann, P., 2013. Tearing and breaking off of subducted slabs as the result of collision of the Panama arc-indenter with northwestern South America Bull, *Seismol. Soc. Am.,* **103**(3) 2025–2046.

Wech, A., Kenneth, W., Creager, C., Houston, H. & Vidale, J., 2010. An earthquake like magnitude–frequency distribution of slow slip in Northern Cascadia, *Geophys. Res. Lett.,* **37,** L22310, doi:10.1029/2010GL044881.

Weingarten, M., Ge, S., Godt, J., Bekins, B. & Rubinstein, J., 2015. High-rate injection is associated with the increase in U.S. mid-continent seismicity, *Science,* **348,** 1336–1344.

Wesnousky, S.G., 1999. *Crustal deformation processes and the stability of the Gutenberg-Richter relationship. Bull. seism. Soc. Am.,* **89** (4),1131–1137.

White, J.A. & Foxall, W., 2016. Assessing induced seismicity risk at CO_2 storage projects: recent progress and remaining challenges, *Int. J. Greenhouse Gas Control,* **49,** 413–424.

Wiemer, S. & Wyss, M., 2000. Minimum magnitude of complete reporting in earthquake catalogs: examples from Alaska, the Western United States, and Japan, *Bull. Seism. Soc. Am.,* **90,** 859–869.

Zang, A., Oye, V., Jousset, P., Deichmann, N., Gritto, R., McGarr, A., Majer, E. & Bruhn, D., 2014. Analysis of induced seismicity in geothermal reservoirs—an overview, *Geothermics,* **52,** 6–21.

Zang, A., Yoon, J.S., Stephansson, O. & Heidbach, O., 2013. Fatigue hydraulic fracturing by cyclic reservoir treatment enhances permeability and reduces induced seismicity, *Geophys. J. Int.,* **195**(2), 1282–1287.